

RESEARCH ARTICLE | NOVEMBER 30 2018

Control of voltage-driven instabilities in cardiac myocytes with memory

Julian Landaw; Zhilin Qu

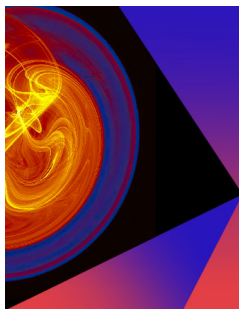


Chaos 28, 113122 (2018)

<https://doi.org/10.1063/1.5040854>




CrossMark



Chaos

Special Topic:
Nonautonomous Dynamical Systems:
Theory, Methods, and Applications

Submit Today

 AIP
Publishing

Control of voltage-driven instabilities in cardiac myocytes with memory

Julian Landaw^{1,2} and Zhilin Qu^{1,2,a)}

¹Department of Medicine (Cardiology), University of California, Los Angeles, California 90095, USA

²Department of Biomathematics, University of California, Los Angeles, California 90095, USA

(Received 21 May 2018; accepted 29 October 2018; published online 30 November 2018)

Sudden cardiac death is known to be associated with dynamical instabilities in the heart, and thus control of dynamical instabilities is considered a potential therapeutic strategy. Different control methods were developed previously, including time-delayed feedback pacing control and constant diastolic interval pacing control. Experimental, theoretical, and simulation studies have examined the efficacy of these control methods in stabilizing action potential dynamics. In this study, we apply these control methods to control complex action potential (AP) dynamics under two diseased conditions: early repolarization syndrome and long QT syndrome, in which voltage-driven instabilities occur in the presence of short-term cardiac memory. In addition, we also develop a feedback pacing method to stabilize these instabilities. We perform theoretical analyses using iterated map models and carry out numerical simulations of AP models. We show that under the normal condition where the memory effect is minimal, all three methods can effectively control the action potential duration (APD) dynamics. Under the two diseased conditions where the memory effect is exacerbated, constant diastolic pacing control is least effective, while the feedback pacing control is most effective. Under a very strong memory effect, all three methods fail to stabilize the voltage-driven instabilities. The failure of effective control is due to memory and the all-or-none AP dynamics which results in very steep changes in APD. *Published by AIP Publishing.* <https://doi.org/10.1063/1.5040854>

Different pacing control methods have been used to control action potential instabilities in cardiac myocytes. In this study, we examine the efficacy of different controlling methods through theoretical analyses and computer simulations in stabilizing voltage-driven instabilities under certain diseased conditions, namely, early repolarization and reduced repolarization reserve. We found that control of the action potential dynamics becomes difficult due to memory and all-or-none action potential dynamics caused by these diseases.

I. INTRODUCTION

Cardiac arrhythmias and sudden cardiac death are known to be associated with dynamical instabilities in the heart.^{1–4} Control of dynamical instabilities in cardiac systems has been widely studied^{5–16} and is considered as a potential therapeutic strategy. Different controlling methods have been proposed and shown to be effective in controlling the instabilities in computer simulations and experiments.

Among the different controlling methods, the method proposed by Hall *et al.*^{9,10} has been widely used,^{12–15} in which a perturbation was applied to the pacing period T , i.e.,

$$T' = T + \frac{\alpha}{2} (a_n - a_{n-1}), \quad (1)$$

where α is the parameter describing the strength of control, and a_n is the action potential duration (APD) of the n^{th} beat. This method is a form of delayed feedback control, which we call *Delayed Negative Feedback Control* (DNFC). Another widely studied method was proposed by Jordan and

Christini¹⁷ and by Wu and Patwardhan,^{18,19} called constant diastolic interval (DI) control, in which the cardiac myocyte or tissue is paced with the DI set as a constant. Recent studies^{20–23} also investigated this method.

In cardiac myocytes, there is a well-known property called APD restitution. In the absence of memory, APD restitution is mathematically described as^{24–26}

$$a_{n+1} = f(d_n) = f(T - a_n), \quad (2)$$

where a_{n+1} is the APD of the $(n+1)^{\text{st}}$ beat and d_n is its immediate preceding DI. It is well known that instabilities can occur when the slope of the APD restitution function is greater than 1. Substituting T by T' in Eq. (2), and performing a linear stability analysis, one obtains the following stability criterion:

$$\frac{f'(d^*) - 1}{f'(d^*)} < \alpha < \frac{2}{f'(d^*)}, \quad (3)$$

where d^* is the steady state DI. In other words, under DNFC, the system is conditionally controllable as long as α is bound by Eq. (3). On the other hand, with constant-DI control, the system is unconditionally controllable since once DI is fixed, then APD is fixed in Eq. (2).

However, it is well known that complex APD dynamics can originate from calcium ion (Ca^{2+})-driven instabilities or the coupling of Ca^{2+} and voltage,^{26,27} and it is understood^{17,28} that constant-DI pacing might fail to control this instability. This is obvious from experiments in which Ca^{2+} alternans occur under voltage or action potential (AP) clamp conditions in which both DI and APD are fixed.^{29–31} In an experimental study,¹⁹ Wu and Patwardhan showed that alternans occurred under both constant-cycle-length pacing and constant-DI pacing, indicating that constant-DI pacing failed to suppress alternans in the real heart. Based on the fact that constant-DI

10 January 2024 05:29:09

^{a)}Electronic mail: zqu@mednet.ucla.edu. URL: <http://cclab.med.ucla.edu>

pacing may stabilize voltage-driven instabilities but may fail in stabilizing Ca^{2+} -driven instabilities, it was proposed to use this method to distinguish voltage-driven instabilities from Ca^{2+} -driven instabilities.²¹

Besides Ca^{2+} -driven instabilities, Eq. (2) does not include memory effects since Eq. (2) assumes that APD depends only on its immediately preceding DI. In the presence of memory, the APD also depends on the previous APDs and DIs, i.e.,

$$a_{n+1} = f(d_n, a_n, d_{n-1}, a_{n-1}, \dots). \quad (4)$$

If one fixes DI by setting $d_n = d_{n-1} = \dots = d_0$, then Eq. (4) becomes

$$a_{n+1} = f(d_0, a_n, a_{n-1}, \dots). \quad (5)$$

In theory, alternans and complex dynamics can still occur in Eq. (2) if the function f exhibits a steep dependence on APD, and thus constant-DI control may fail to stabilize voltage-driven instabilities in the presence of memory. It is also not clear how effective are the other control methods, such as the DNFC method, in controlling the APD dynamics in the presence of memory.

Most of the previous studies on the cardiac memory effect^{12,32–43} showed that memory itself suppresses voltage-driven instabilities, but studies have also shown that memory may promote APD instabilities.^{33,44} If memory suppresses APD instabilities, then it is not difficult to imagine that control may become easier in the presence of memory. However, a recent study by Otani²² discussed the possibility of constant-DI pacing failure in controlling the voltage-driven instabilities if a steep APD dependence on the memory variable exists. As shown in a study by Sun *et al.*,⁴⁴ the presence of memory drives alternans and more complex behaviors in AV nodal conduction. Our recent studies^{45,46} showed that the steep dependence can indeed exist under certain diseased conditions, i.e., the all-or-none behaviors caused by the diseases result in steep APD dependence on the memory variables, which causes complex APD dynamics.

In this study, we investigate the efficacy of the DNFC method and the constant-DI pacing control in controlling the voltage-driven instabilities under two diseased conditions in which the memory effect is exacerbated. We also propose a simple feedback pacing control method to control instability which we call *Negative Feedback Control* (NFC). The first diseased condition is called early repolarization which occurs in Brugada syndrome, J-wave syndrome, and short QT syndrome.⁴⁷ In this case, enhanced outward currents and/or reduced inward currents cause an abrupt shortening in APD. The second diseased condition is reduced repolarization reserve which occurs in long QT syndrome^{48,49} and heart failure.^{50–52} In this case, enhanced inward currents and/or reduced outward currents promote early afterdepolarizations (EADs), causing an abrupt lengthening in APD. In both cases, the steep APD response combined with the memory effect results in complex APD dynamics, which are purely voltage-driven instabilities.^{45,46} We show that under normal conditions in which the memory effect is minimal, all three controlling methods can effectively stabilize instabilities caused by steep APD restitution. However, under diseased conditions,

constant-DI pacing control is the least effective controlling algorithm, almost completely failing to stabilize the APD. The DNFC method can stabilize the instabilities for a certain pacing period T with properly control strength α , but fails to eliminate instabilities. In other words, even for an optimal α , complex APD dynamics still occurs for certain pacing periods. The NFC method is most effective, which can eliminate instabilities for a certain range of control strength α . Under a very strong memory effect, all three methods fail. We demonstrate these results using computer simulations of AP models and theoretical analyses of iterated map models. Our results imply that under these diseased conditions, pacing control may only be marginally effective in stabilizing the voltage-driven instabilities due to memory and the steep APD response arising from all-or-none behaviors.

II. METHODS

We carry out computer simulations using two AP models with the voltage (V) governed by the following differential equation:

$$C_m \frac{dV}{dt} = -I_{ion} + I_{sti}, \quad (6)$$

where $C_m = 1 \mu\text{F}/\text{cm}^2$ is the membrane capacitance, I_{ion} is the total ionic current density, and I_{sti} is the stimulus current density applied for a given duration.

The first action potential model we use is the phase I Luo and Rudy (LR1) 1991 model,⁵³ which is one of the simplest cardiac AP models with physiological ionic current formulations. Since there is no I_{to} in the LR1 model, to model the condition of early repolarization or Brugada syndrome, we add an I_{to} to it, which is the formulation of the fast I_{to} (i.e., $I_{to,f}$) from the model by Mahajan *et al.*⁵⁴

$$I_{to} = g_{to} x_{to} y_{to} (V - E_K), \quad (7)$$

where g_{to} is the maximum I_{to} conductance, x_{to} is the activation gating variable, y_{to} is the inactivation gating variable, and E_K is the reversal potential of K^+ . In this model, the pacing stimulus we use is $I_{sti} = 80 \mu\text{A}/\text{cm}^2$ for a 0.5 ms duration. With the addition of I_{to} , we refer to this model as the *LR1+ I_{to} model*. We set $g_{to} = 0.21 \text{ mS}/\text{cm}^2$ and make the following parameter and model changes:⁴⁵ $G_{si} = 0.1035 \text{ mS}/\text{cm}^2$, $G_{K1} = 0.133034 \text{ mS}/\text{cm}^2$, the voltage-dependent time constant of the X -gating variable of I_K is increased 5-fold ($\tau_X \rightarrow 5\tau_X$), and the steady-state curve of $y_{to,f}$ is shifted by 8 mV to more positive voltages.

We also use our recently developed iterated map model that incorporates memory from the slow K^+ channel recovery^{45,46} to investigate the efficacy of the different control methods. The model is described by the following equations:

$$x_{n+1} = w(x_n, a_n, d_n) = \left[x_a - (x_a - x_n) e^{-\frac{a_n}{\tau_a}} \right] e^{-\frac{d_n}{\tau_d}}, \quad (8)$$

$$a_n = g(x_n), \quad (9)$$

$$d_n = p(a_n) = mT - a_n, \quad (10)$$

where x_n is the variable describing the memory effect from the slow recovery of the K^+ channel, more specifically the

X-gating variable of I_K in the LR1 model. The function g describes the dependence of APD on the memory variable X . In this paper, we assume that $m = 1$, so there is always 1:1 capture. We call this model the *X-memory map model*. In our previous studies,^{45,46} we determined parameter values $x_a = 0.6$, $\tau_a = 3000$ ms, and $\tau_d = 1000$ ms to match closely with the results seen in the LR1+ I_{to} model. The function g was determined by simulating the LR1+ I_{to} model at a fixed pacing period $T = 1500$ ms, and at the time of the last stimulus the value of X is changed to a new value x_{init} . The APD of the resulting AP is then recorded for different values of x_{init} . The dependence of APD on x_{init} is shown in Fig. 1(f), and a linear interpolation of the data is used for g in the X-memory map model [Eq. (9)].

The second AP model we use is a much more complex one, a human ventricular AP model developed by ten Tusscher *et al.*,⁵⁵ denoted as the *TP04 model* in this study. I_{to} formulations (both slow and fast I_{to}) are present in the TP04 model, so for simplicity and consistency we remove the two original I_{to} formulations and add the I_{to} formulation in Eq. (7). In this model, the stimulus current is $I_{sti} = 52 \mu\text{A}/\text{cm}^2$ for a 1 ms duration.

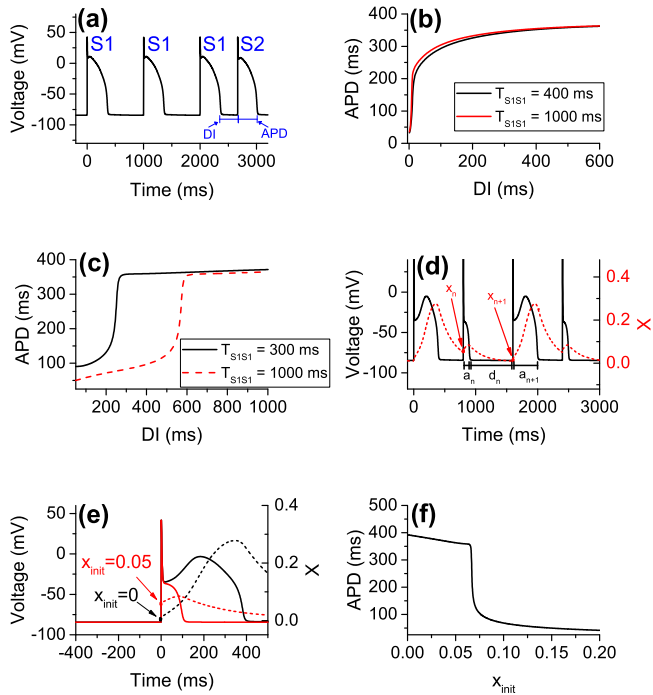


FIG. 1. The S1S2 APD restitution and memory. (a) Schematic plot of the S1S2 pacing protocol. A cell is paced with an S1-pacing period T , followed by a premature stimulus (S2) after a given DI, and the resulting APD is recorded. (b) S1S2 APD restitutions of the LR1 model without I_{to} for S1-pacing periods: $T = 400$ ms and 1000 ms. (c) S1S2 APD restitutions of the LR1+ I_{to} model for S1-pacing periods: $T = 300$ ms and 1000 ms. (d) Action potentials of the LR1+ I_{to} model plotted against the gating variable X during APD alternans. (e) Effects of initial X values, x_{init} , on APD. When $x_{init} = 0$, the resulting AP has a spike-and-dome with a prolonged APD. When $x_{init} = 0.05$, the resulting AP has a spike with a shortened APD. (f) Plot of APD against x_{init} . The curve was generated by simulating the LR1+ I_{to} model at a fixed pacing period $T = 1500$ ms, and at the time of the next stimulus the value of X is changed, as illustrated in (e). The resulting APD is then recorded. This curve is used as the function g in the X-memory map model [Eq. (9)].

Since memory in the TP04 model is mainly caused by slow intracellular ion concentration accumulation, we previously developed another iterated map model to describe its memory effects and dynamics,⁴⁶ which is described by the following equations:

$$c_{n+1} = w(c_n, a_n, T) = c_n e^{\gamma_a a_n - \gamma_T T + \delta}, \quad (11)$$

$$a_n = g(c_n), \quad (12)$$

$$d_n = mT - a_n, \quad (13)$$

where Eq. (11) is the iterated map describing the memory effect from the slow accumulation of the intracellular Ca^{2+} concentration. We refer to this model as the *Ca^{2+} -memory map model*. Note that under constant- T pacing with 1:1 capture ($m = 1$), $T = a_n + d_n$, so Eq. (11) becomes $c_{n+1} = w(c_n, a_n, d_n) = c_n e^{(\gamma_a - \gamma_T) a_n - \gamma_T d_n + \delta}$. The results from simulations of the TP04 model and of the Ca^{2+} -memory map model are in the [supplementary material](#). In our previous study,⁴⁶ we determined parameter values $\gamma_a = 2 \times 10^{-4} \text{ms}^{-1}$, $\gamma_T = 3.625 \times 10^{-6} \text{ms}^{-1}$, and $\delta = -0.0275$.

Numerical simulations of the AP models are carried out using an adaptive forward-Euler method in which the time step $\Delta t = 0.05$ ms. If at any step the change in voltage would be greater than 0.1 mV, i.e., $\Delta V > 0.1$ mV, the time step is then $\Delta t = 0.005$ ms. For every AP, the APD is calculated to be the duration of time such that $V > -75$ mV.

III. RESULTS

A. Stability analysis of a general iterated map model

To analyze in general the APD stability of the system under different control methods, we consider the following general iterated map model, similar to the method used by Otani:²²

$$z_{n+1} = w(z_n, a_n, d_n), \quad (14)$$

$$a_n = g(z_n), \quad (15)$$

$$d_n = p(a_n, a_{n-1}, \dots). \quad (16)$$

Both the X-memory map model [Eqs. (8)–(10)] and the Ca^{2+} -memory map model [Eqs. (11)–(13)] are specific applications of the general iterated map model. The function $w = w(z, a, d)$ determines the growth or decay of the memory variable z dependent on the previous beat's APD (a) and DI (d). For example, in the LR1+ I_{to} model, the memory variable X activates (increases) during the APD and deactivates (decreases) during the DI. The dotted-red curve in Fig. 1(d) shows that between x_n and x_{n+1} , the APD is short and the DI is long, resulting in a net decrease in X and thus $x_{n+1} < x_n$. Equations (8) and (11) provide explicit expressions for w in the X-memory map model and the Ca^{2+} -memory map model, respectively. For the X-memory map model, $z = x$, and for the Ca^{2+} -memory map model, $z = c$. The function g determines the dependence of APD on the memory variable.

The function p determines the method of “control,” which is a constant for constant-DI control or a function of APD for the other control methods. In other words, p determines the

period of time between repolarization of the previous AP and the next stimulus. Different control methods have p depending on a variable number of prior APDs. For example, in constant-DI control, $d_n = d_0$ so p is a constant independent of APD.

Together, Eqs. (14)–(16) simplify to

$$\begin{aligned} a_{n+1} &= g(z_{n+1}) = g(w[g^{-1}(a_n), a_n, p(a_n, a_{n-1}, \dots)]) \\ &\equiv H(a_n, a_{n-1}, \dots), \end{aligned} \quad (17)$$

so a_{n+1} depends explicitly on prior APDs via the map H . The dimensionality of the iterated map depends on the control function p . If p is constant or depends on only the previous APD a_n , then Eq. (17) is 1-dimensional. If, however, p depends on the previous $m > 1$ APDs so that $p = p(a_n, a_{n-1}, \dots, a_{n-m+1})$, then Eq. (17) is an $(m-1)$ -dimensional iterated map.

Under constant-T pacing, the n^{th} DI satisfies

$$d_n = p(a_n) = T - a_n. \quad (18)$$

Since $p = p(a_n)$ depends only on the prior APD, the return map H in Eq. (17) is 1-dimensional. Denoting the return map under constant-T pacing as H_T , the APD fixed point as a^* , and $z^* = g^{-1}(a^*)$ the corresponding memory fixed point, then the derivative of the iterated map at the fixed point is

$$\begin{aligned} H'_T &\equiv H'_T(a^*) = \frac{\partial w}{\partial z} + g'(z^*) \left(\frac{\partial w}{\partial a} - \frac{\partial w}{\partial d} \right) \\ &= \rho - \sigma (\xi + \omega), \end{aligned} \quad (19)$$

where

$$\sigma = -g'(z^*), \quad \rho = \frac{\partial w}{\partial z}, \quad \xi = \frac{\partial w}{\partial a}, \quad \omega = -\frac{\partial w}{\partial d}. \quad (20)$$

σ measures the dependence of APD on the memory variable z , and ω measures how slowly z changes during the DI. We make a number of constraints on the variables ρ , ξ , and ω to be physiologically realistic. First, $\omega > 0$ (i.e., $\frac{\partial w}{\partial d} < 0$) since the memory variable decays during the DI. For example, the X-gating variable of I_{Ks} deactivates during the DI, and Ca^{2+} is effluxed out of the cytoplasm during the DI via the sodium-calcium exchanger (NCX). Similarly, $\xi > 0$ since the memory variable accumulates in the DI. For example, the X-gating variable activates during the AP, and Ca^{2+} accumulates in the cytoplasm via the calcium window current (I_{CaL}) and the SERCA pump during the AP. Finally, ρ must be constrained to $|\rho| < 1$, so that when the APD and DI are fixed, z stabilizes to z^* . In other words, restraining $|\rho| < 1$ assures that when voltage is stable, e.g., under voltage clamp conditions, memory is also stable. We are primarily interested in how σ and ω —the APD dependence on memory and the kinetics of memory—determine APD instability under constant-T pacing and under control. Thus, we consider ρ and ξ as fixed constants. For the DNFC and NFC methods, we are also interested in α , which determines the strength of the two control schemes.

Under constant-T pacing, the APD fixed point is stable when $|H'_T(a^*)| < 1$, which leads to

$$\frac{\rho - 1}{\xi + \omega} < \sigma < \frac{\rho + 1}{\xi + \omega}. \quad (21)$$

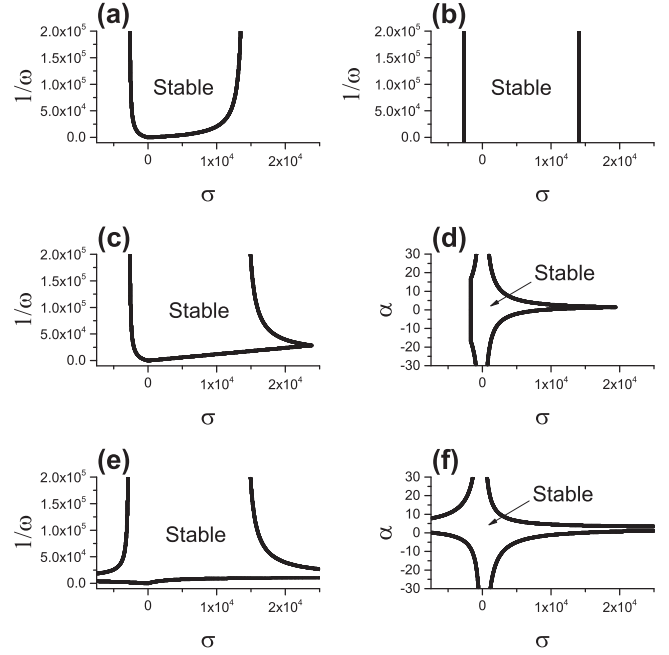


FIG. 2. Stability of constant-T pacing (a) constant-DI pacing (b) DNFC [(c) and (d)] and NFC [(e) and (f)] dependent on the parameters $\sigma = -g'(z^*)$, $\omega = -\frac{\partial w}{\partial d}$, and α . We set $\rho = 0.67368$ and $\xi = 1.190168 \times 10^{-4}$ fixed, which match closely to the simulation results of the LR1+ I_{to} model with $T = 515$ ms. In panels (c) and (e), we fix $\alpha = 2.4$; in panels (d) and (f), we fix $\omega = 7 \times 10^{-5}$, which also matches closely to the simulation results of the LR1+ I_{to} model with $T = 515$ ms.

For illustrative purposes, we provide an example stability region of σ and ω in Fig. 2(a) for fixed values of ρ and ξ . The stability boundary lines $\sigma = (\rho \pm 1)/(\xi + \omega)$ are plotted. The APD fixed point is stable under constant-T pacing provided σ is not too large (or too negative). A smaller ω tends to help stability but only to an extent. In particular, if $\sigma > (\rho + 1)/\xi$ then the fixed point will always be unstable, independent of ω .

Under constant-DI pacing, $d_n = d_0$, so the function p in Eq. (16) is a constant independent of prior APDs and the return map is 1-dimensional. Denoting the return map under constant-DI pacing as H_{DI} , then its derivative evaluated at the APD fixed point is

$$H'_{DI} \equiv H'_{DI}(a^*) = \rho - \sigma \xi. \quad (22)$$

Note that $H'_{DI} = H'_T + \sigma \omega$. Constant-DI pacing will stabilize the APD fixed point provided

$$\frac{\rho - 1}{\xi} < \sigma < \frac{\rho + 1}{\xi}. \quad (23)$$

This stability criterion is nearly identical to the constant-T pacing stability criterion [Eq. (21)], but the ω term in the denominators is absent here. The inequalities in Eq. (23) are independent of ω , and so stability depends solely on σ . Namely, if σ is too large (or too negative), constant-DI pacing will fail to stabilize the fixed point. In Fig. 2(b), the boundary lines $\sigma = (\rho \pm 1)/\xi$ are plotted. Compared to the stability region for constant-T pacing [Fig. 2(a)], constant-DI pacing is more stable, but the effectiveness of constant-DI pacing diminishes as ω gets smaller. More specifically, the upper stability limit of σ for constant-T pacing is $(\rho + 1)/(\xi + \omega)$ compared to $(\rho + 1)/\xi$ for constant-DI pacing. In the region

$(\rho + 1)/(\xi + \omega) < \sigma < (\rho + 1)/\xi$, constant-DI pacing will stabilize the fixed point where constant-T pacing fails, and this region shrinks as ω gets small. In the presence of memory, constant-DI pacing no longer stabilizes the fixed point unconditionally, and its efficacy of control may strongly depend on the memory effect, despite the fact that the APD instability is completely voltage driven.

Next, we consider the effectiveness of the DNFC method. Under the DNFC method, the pacing period T changes to a new pacing period T' , as described in Eq. (1). Setting $d_n = T' - a_n$ in Eq. (1) gives

$$d_n = p(a_n, a_{n-1}) = T - a_n + \frac{\alpha}{2}(a_n - a_{n-1}). \quad (24)$$

Note that setting $\alpha = 0$ is equivalent to constant-T pacing. Under steady state $d_n = d^* = T - a^*$, so $T = a^* + d^*$ is the steady state pacing period.

Because $p = p(a_n, a_{n-1})$ depends on the prior two APDs, the iterated map in Eq. (17) is 2-dimensional such that a_{n+1} depends on both a_n and a_{n-1} . The Jacobian of the iterated map under DNFC is

$$J_{DNFC} \equiv \begin{pmatrix} \rho - \sigma \left[\xi + \frac{(2-\alpha)\omega}{2} \right] & -\frac{\alpha\sigma\omega}{2} \\ 1 & 0 \end{pmatrix}. \quad (25)$$

The fixed point is stable if and only if the two eigenvalues of J_{DNFC} have magnitude less than 1. This leads to the following stability criteria:

$$-2 < \sigma(\xi + \omega) - \rho - 1 < \alpha\sigma\omega < 2. \quad (26)$$

All three inequalities in Eq. (26) have to be met to guarantee stability. Figures 2(c) and 2(d) show the boundaries of the stability region of the DNFC method for α fixed, varying σ and ω [panel (c)] and for ω fixed, varying σ and α [panel (d)]. If σ is sufficiently large such that $\sigma > \frac{\rho+3}{\xi+\omega}$, the DNFC method will always fail to stabilize the APD fixed point. This condition is equivalent to $H'_T < -3$ so that if the derivative of the iterated map under constant-T pacing is sufficiently negative (less than -3), the DNFC method will always fail to stabilize the fixed point. In Fig. 2(c), for a fixed α , the curves $\sigma(\xi + \omega) - \rho - 1 = \alpha\sigma\omega$ and $\alpha\sigma\omega = 2$ meet at the point $(\sigma, \omega) = \left(\frac{\rho+3-\frac{2}{\alpha}}{\xi}, \frac{2\xi}{\alpha(\rho+3)-2} \right)$, and choosing $\alpha = (2\xi + 2\omega)/(\omega(\rho + 3))$ will maximize the range of σ that will stabilize the fixed point. This value of α is precisely the point of the cusp seen in Fig. 2(d), where the fixed point is stable up to $\sigma \approx 2 \times 10^4$. However, despite the limitations of the DNFC method, the method is in general superior to constant-T and constant-DI pacing, as the region of stability increases (as long as α is chosen appropriately). For example, under constant-T pacing the fixed point is stable provided $\sigma < (\rho + 1)/(\xi + \omega)$, whereas the DNFC method can stabilize the fixed point so long as $\sigma < (\rho + 3)/(\xi + \omega)$.

Finally, we consider NFC. This is a new control method we propose in this study in which the pacing period T is perturbed by the following equation:

$$T' = T + \alpha(a_n - a^*), \quad (27)$$

where a^* is the APD fixed point under constant-T pacing. This is a form of negative feedback control. For example, under APD alternans, if $a_n > a^*$ so that a_{n+1} would be smaller than

a^* , then the pacing period is lengthened to facilitate a_{n+1} to be closer to a^* . Conversely, if $a_n < a^*$ so that a_{n+1} would be larger than a^* , the pacing period is shortened to decrease a_{n+1} and be closer to a^* . Setting $d_n = T' - a_n$ gives

$$d_n = p(a_n) = T - a_n + \alpha(a_n - a^*). \quad (28)$$

Note that Eq. (28) is equivalent to $d_n = \kappa_0 + (\alpha - 1)a_n$ where $\kappa_0 = T - \alpha a^*$. Although the APD fixed point a^* may not be known in advance in Eq. (28), κ_0 may be varied freely. Setting $\alpha = 0$ is equivalent to constant-T pacing, and setting $\alpha = 1$ is equivalent to constant-DI pacing [since $d_n = T - a_n + 1 \cdot (a_n - a^*) = T - a^*$ is a constant independent of a_n].

Because $p = p(a_n)$ depends only on the previous APD, the iterated map is 1-dimensional. Denoting H_{NFC} as the APD return map under NFC control, then its derivative is

$$H'_{NFC} \equiv H'_{NFC}(a^*) = \rho - \sigma[\xi + (1 - \alpha)\omega]. \quad (29)$$

Stability of the fixed point is satisfied provided

$$\rho - 1 < \sigma[\xi + (1 - \alpha)\omega] < \rho + 1. \quad (30)$$

See Figs. 2(e) and 2(f) for an example stability region under NFC. In contrast to the DNFC method, the NFC method can always stabilize the system provided a proper α is chosen. In particular, setting $\alpha = 1 + \xi/\omega - \rho/(\sigma\omega) \equiv \bar{\alpha}$ makes $H'_{NFC} = 0$ and the fixed point is stable regardless of how large or small σ and ω are. However, the range of α that stabilizes the fixed point may be very narrow so that stability is very sensitive to the exact choice of α . In particular, the fixed point is stable provided $|\alpha - \bar{\alpha}| < 1/(\sigma\omega)$, and so when σ gets large the range of α that stabilizes the fixed point gets narrower.

We have established the stability criteria of the APD fixed point under constant-T pacing [Eq. (21)], constant-DI pacing [Eq. (23)], DNFC [Eq. (26)], and NFC [Eq. (30)]. Among all control methods, NFC is most effective at stabilizing the APD fixed point, and in particular is the only method that can stabilize the fixed point regardless of the parameters of the iterated map. However, there are still limitations, namely that if σ is sufficiently large so that $\sigma \gg \frac{1}{\omega}$, then the stability of the fixed point is very sensitive on the NFC parameter α . In other words, a small deviation from an optimal α that stabilizes the fixed point may destabilize the fixed point.

In Secs. III B and III C, we carry out computer simulations using iterated map models and AP models to examine the general theoretical predictions of the efficacy of the three control methods.

B. Controlling voltage-driven instabilities due to slow K^+ channel deactivation in the presence of I_{to}

1. Constant-T vs. Constant-DI pacing

For both the LR1 and LR1+ I_{to} models, we perform constant-T and constant-DI pacing under various pacing periods and DIs and plot the corresponding APDs. Bifurcation diagrams are shown in Fig. 3. Without I_{to} , the system is unstable under very fast pacing [$T < 300$ ms—see Fig. 3(a)]. The constant-DI method is able to completely stabilize the system [see Fig. 3(b)]. This is because the S1S2 APD restitution of

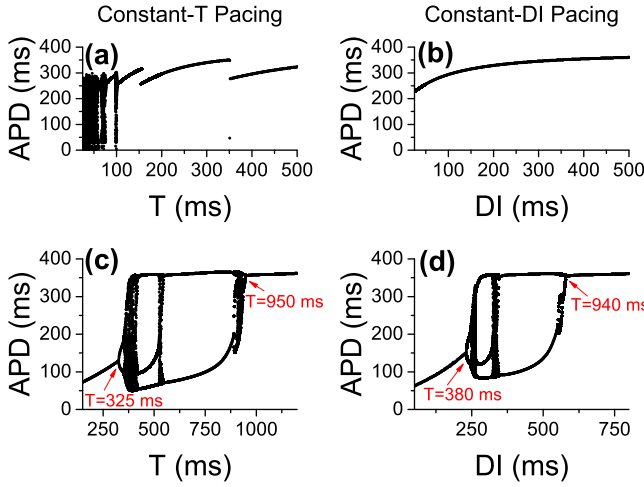


FIG. 3. APD bifurcation diagrams of the LR1 (first row) and LR1+ I_{to} (second row) models under constant-T pacing (left panels) and constant-DI pacing (right panels).

the LR1 model has minimal dependence on prior pacing periods, i.e., the memory effect is minimal so that APD depends mainly on the immediate preceding DI [see Fig. 1(b)].

In the LR1+ I_{to} model, instability occurs at much slower pacing periods [see Fig. 3(c)], and there is a period-doubling bifurcation route to enter and exit chaos around pacing periods $T = 325$ ms and $T = 950$ ms. In this scenario, constant-DI pacing fails to stabilize the system for most pacing periods [see Fig. 3(d)]. The region of instability does shrink, as constant-DI control stabilizes APD instability around the pacing periods between 325 and 380 ms and between 940 and 950 ms. However, the constant-DI method fails to stabilize the system for the pacing periods between 380 and 940 ms. This agrees with the general theoretical analysis above that constant-DI pacing can only stabilize a small range of parameters when the memory effect is large. Figure 4 shows two examples, one in which constant-DI pacing does successfully stabilize APD dynamics ($T = 373$ ms) and on which constant-DI pacing fails to stabilize ($T = 515$ ms).

Findings from the X-memory map model are consistent with the simulation results of the LR1+ I_{to} model. From Eq. (8), we have

$$\sigma = -g'(x^*), \quad \omega = \frac{x^*}{\tau_d}. \quad (31)$$

From Sec. II, we have shown that in general, constant-DI pacing is more stable compared to constant-T pacing. However, the efficacy of constant-DI pacing depends on σ and ω . As we have shown, constant-T pacing is unstable if $\sigma > (\rho + 1)/(\xi + \omega)$, while constant-DI pacing is stable when $\sigma < (\rho + 1)/\xi$. Therefore, when APD has too steep dependence on memory (σ large) and/or the system has a long memory (ω small), constant-DI pacing control may fail.

Figure 5 shows the bifurcation diagrams of APD dynamics of the X-memory map model under both methods of pacing. We used a g -function that was measured from the LR1+ I_{to} model using the same parameters as for Fig. 4 [i.e., the curve shown in Fig. 1(f)]. For a narrow range of pacing periods (396–438 ms and 990–1000 ms), constant-DI pacing

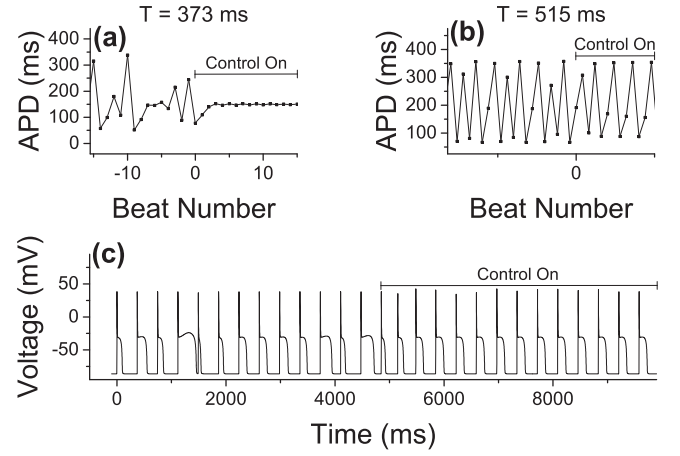


FIG. 4. Dynamics of the LR1+ I_{to} model when switching between constant-T pacing and constant-DI pacing. (a) APD vs. beat number for $T = 373$ ms. At beat number 0, the system switches from constant-T pacing to constant-DI pacing. After about 5 beats, the APD is stabilized to about 150 ms. (b) APD vs. beat number for $T = 515$ ms. Constant-DI pacing switches the chaotic APD dynamics to period-3, failing to stabilize the system. (c) APs before and after the switch from constant-T pacing to constant-DI pacing for $T = 373$ ms, leading to stable APs.

stabilizes APD. However, for most pacing periods (438–990 ms), constant-DI pacing fails to stabilize APD. These results agree well with the simulation results of the LR1+ I_{to} model shown in Figs. 4(c) and 4(d). The failure of constant-DI pacing in stabilizing the fixed point is because σ is too large. Based on Fig. 1(f), the maximum value of σ , i.e., the maximum slope of the curve in Fig. 1(f), is 1.5×10^5 , which is much larger than the critical σ shown in Fig. 2(b).

2. The DNFC method

We next simulate the LR1+ I_{to} model with the DNFC method, and the results are shown in Fig. 6. Figure 6(a) shows the stability region of the model for various values of pacing period T and DNFC parameter α . The DNFC method can stabilize the model at some pacing periods, but for pacing periods in the range of 400–900 ms the DNFC method fails to stabilize the fixed point. Figure 6(b) shows a bifurcation diagram of the model when $\alpha = 1$, indicating that though the instability region has shrunk compared to constant-T pacing [as in Fig. 5(a)], there is still a period-doubling bifurcation route to enter and exit chaos. Figure 6(c) shows an example of APD dynamics when the DNFC method does work at $T = 373$ ms, whereas Fig. 6(d) shows that the DNFC method fails when $T = 515$ ms.

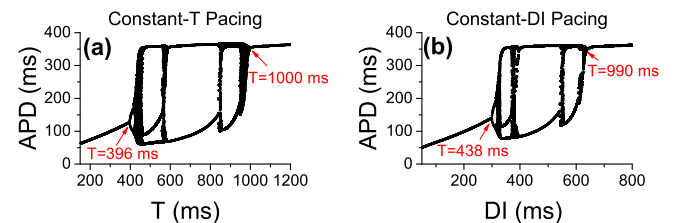


FIG. 5. APD dynamics of the X-memory map model in Eqs. (8)–(10) under (a) constant-T pacing and (b) constant-DI pacing. Arrows point to the bifurcation points.

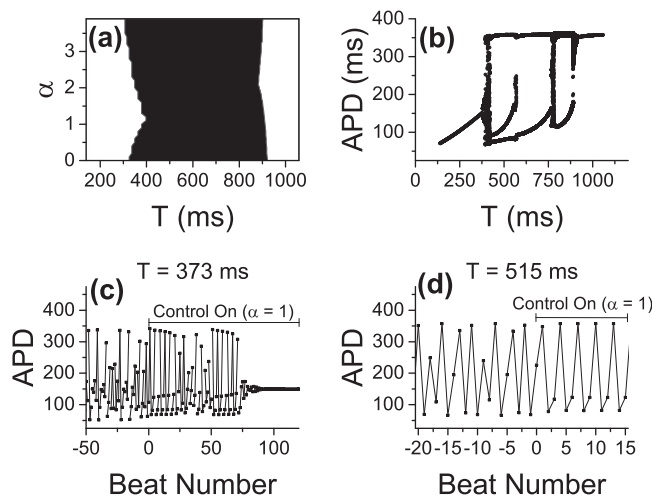


FIG. 6. APD dynamics of the LR1+ I_{to} model when implementing the DNFC method. (a) Stability region of the model for different values of pacing period T and DNFC parameter α . (b) Bifurcation diagram with $\alpha = 1$. (c) APD vs. beat number setting $T = 373$ ms. The DNFC method begins at beat number 0, and before that the model is paced with constant- T pacing. The model stabilizes to a fixed APD after about 100 APs. (d) APD vs. beat number setting $T = 515$ ms. The DNFC method fails to stabilize.

Using the X -memory map model [Eqs. (8)–(10)], Fig. 7 shows the stability region of the DNFC method of the iterated map. For some pacing periods, the DNFC method can successfully stabilize APD dynamics. Up to $\alpha = 1.5$, the region of instability decreases to pacing periods between 500 and 980 ms. For pacing periods between 396 and 500 ms the DNFC method is effective and can stabilize APD dynamics. However, when α is too large (e.g., $\alpha > 1.5$), the APD fixed point becomes unstable again. The shape of the instability region is very similar to that seen in the LR1+ I_{to} model in Fig. 6(a). The iterated map model can well capture the behavior of the action potential model.

3. The NFC method

Finally, we perform simulations of the LR1+ I_{to} model under the NFC method. The results are shown in Fig. 8. As shown in Fig. 8(a), APD dynamics can be stabilized for every pacing period by the NFC method for a sufficient choice of α . When α is too large, the ionic model becomes unstable again. This is consistent with our prior stability analysis and criterion in Eq. (30). Figure 8(b) shows APD dynamics before and after implementation of the NFC method with $T = 515$ ms. With

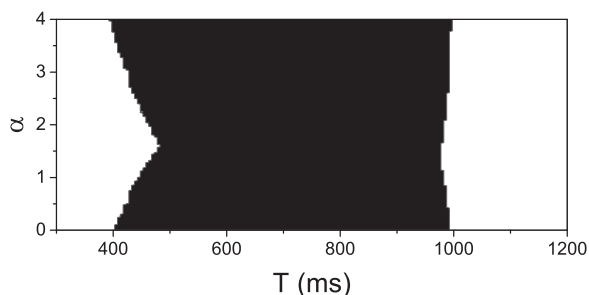


FIG. 7. Stability region of the X -memory map model [Eqs. (8)–(10)] when implementing the DNFC method [Eq. (24)]. The dark region is where the APD fixed point is unstable.

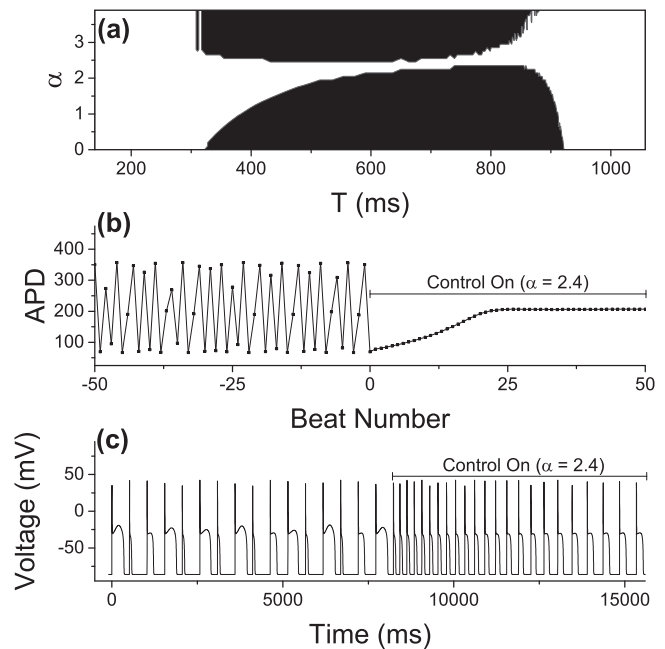


FIG. 8. APD dynamics of the LR1+ I_{to} model using the NFC method. (a) Stability region for various values of pacing period T and NFC method parameter α . The dark region is where the APD fixed point is unstable. (b) APD vs. beat number before and after the NFC method is implemented with $\alpha = 2.4$ and $T = 515$ ms. Once the control method is implemented, it takes about 25 APs before the APD stabilizes to 180 ms. (c) APs before and after the NFC method is implemented, corresponding to the data shown in panel (b).

constant- T pacing, the APDs are undergoing chaotic dynamics. When the NFC method is implemented with $\alpha = 2.4$, the APD slowly increases from one beat to the next until the APD stabilizes to about 180 ms. The APs of this behavior is shown in the next panel, Fig. 8(c).

We next consider the regions of stability of the NFC method using the X -memory map model [Eqs. (8)–(10)]. The results are shown in Fig. 9. Consistent with the stability criterion in Eq. (30), every pacing period T can be stabilized by the NFC method using some choice of α . In fact, there is a very narrow choice around $\alpha = 2.4$ which will stabilize APD dynamics for all pacing periods. For $\alpha > 2.4$, a new region of instability emerges. These results are consistent with our prior analysis that although the NFC method can successfully stabilize APD dynamics, the range of α can be quite narrow. As we have shown, this range depends on $1/(\sigma\omega)$, and so with σ sufficiently large the map is stable for only a narrow range of α .

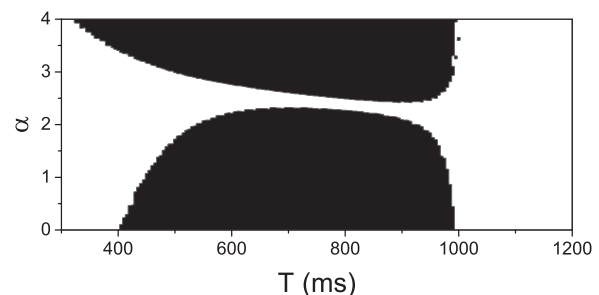


FIG. 9. Stability region of the X -memory map model [Eqs. (8)–(10)] under the NFC method [Eq. (28)]. The x -axis is the pacing period T , and the y -axis is the control parameter α . The dark region is where the APD fixed point is unstable.

C. Efficacy of controlling voltage instabilities due to ion concentration accumulation

As shown in our previous work,⁴⁶ in the TP04 model, slow Ca^{2+} concentration accumulation causes APD dynamics and instability. APD depends very sensitively on Ca^{2+} , and Ca^{2+} concentration equilibrates with a time constant on the order of several seconds. In contrast, the X -gating variable in the $\text{LR1}+I_{to}$ model equilibrates with a time constant of about 1 s.

Controlling APD instability proves very difficult in the TP04 model and the Ca^{2+} -memory map model [Eqs. (11)–(13)]. As we have shown previously,⁴⁶ the Ca^{2+} -memory map model can accurately capture the bifurcations of the TP04 model. Here, we only evaluate the efficacy of the control methods using the iterated map model. Bifurcation diagrams and stability maps of the Ca^{2+} -memory map model under the different control methods are shown in Figs. S3–S5 in the [supplementary material](#) section. Under constant-T pacing, APDs are unstable for all pacing periods up to $T = 8420$ ms. The constant-DI method fails to control instabilities for nearly all pacing periods, with the exception of a small range of pacing periods between 8410 and 8420 ms (Fig. S3). This is due to the fact that in the model, ω is very large and so constant-DI pacing is only effective in a very narrow range.

The DNFC method also has limited efficacy, only successfully stabilizing APD dynamics under rapid pacing (Fig. S4). The NFC method is able to successfully stabilize APDs, but only when the NFC control parameter is in a very narrow range around $\alpha = 55.1$ (Fig. S5). The controllability of APD dynamics under the Ca^{2+} -memory map model is incredibly sensitive to changes in α ; for example, setting $\alpha = 55$ instead of 55.1 fails to stabilize APD dynamics for most pacing periods [Fig. S5(b)]. The range of α that stabilizes the iterated map depends on $1/(\sigma\omega)$, and since σ is very large, stability is very sensitive on α .

D. Efficacy of controlling voltage instabilities induced by EADs

As shown previously,^{45,46} we use the LR1 model and modify I_K by increasing the voltage-dependent time constant of the X -gating variable 10-fold ($\tau_X \rightarrow 10\tau_X$) to promote EADs. Using our X -memory map model in Eqs. (8)–(10), with parameter values $x_a = 0.6$, $\tau_a = 6000$ ms, and $\tau_d = 2000$ ms, we can well capture the bifurcations of the LR1 model in the presence of EADs. Again, we can use this iterated map to evaluate the efficacy of the different control methods on stabilizing the fixed point. The function g was determined in exactly the same fashion as the function g was determined using the $\text{LR1}+I_{to}$ model, but instead using the LR1 model in the presence of EADs.

Bifurcation diagrams and stability maps of the iterated map model under the different control methods are provided in Figs. S6 and S7. Under constant-T pacing at $T = 1250$ ms, a period-doubling bifurcation point occurs where the APs are stable with 0 EADs ($T < 1250$ ms) to complex APD alternans ($T > 1250$ ms) soon leading to complex APD dynamics with EADs [Fig. S6(a)]. Under constant-DI pacing [Fig. S6(b)],

the bifurcation point shifts slightly to $T = 1280$ ms, and so constant-DI pacing successfully stabilizes APD dynamics for pacing periods between 1250 and 1280 ms. However, the method fails to control APD dynamics under all pacing periods greater than 1280 ms.

The DNFC and NFC methods have little success in controlling APD instability (Fig. S7). As shown in Fig. S7(a), the DNFC method has limited success to control instability up to $\alpha = 1$ near the bifurcation point around $T = 1250$ ms and at the bifurcation points corresponding to transitions from 1 EAD to 2 EADs ($T = 1750$ ms) and from 2 EADs to 3 EADs ($T = 2050$ ms). As expected, the NFC method [Fig. S7(b)] does successfully stabilize APD dynamics, but under very narrow choices of α around $\alpha = 1.6$.

IV. DISCUSSION AND CONCLUSIONS

In this study, we investigated the efficacy of three pacing control methods in stabilizing voltage-driven instabilities in ventricular myocytes under two diseased conditions. The three control methods include two previous widely studied methods^{9,10,17} and a new one proposed in this study. We show that under the normal condition in which there is no or little memory effect, all three methods can successfully stabilize the voltage-driven instabilities caused by steep APD restitution curves. However, under the two diseased conditions, constant-DI pacing almost completely fails to stabilize the voltage-driven instabilities, while the other two methods can suppress the instabilities with the simple feedback pacing being the most effective. Note that in the absence of the memory effect [Eq. (2)], under constant-DI pacing, the system is unconditionally controllable, while under the other two methods, the system is conditionally controllable. The failure of constant-DI pacing in stabilizing voltage-driven instabilities agrees with the prediction by Otani²² using a generic iterated map model. The controllability of the system depends on the strength of the memory effect and the steepness of the APD dependence on the memory variables. As shown by Hall *et al.*¹⁰ who used an experimental model in which alternans was likely promoted by the memory effect,⁴⁴ alternans can be controlled by the time-delayed feedback pacing algorithm. As shown in this study, under the diseased conditions, the strong memory effect and the all-or-none behaviors make the controlling to be difficult. Moreover, the instabilities tend to occur at multiple scales with multiple causes and mechanisms,⁵⁶ one would expect that more sophisticated controlling methods are needed to control the instabilities under the diseased conditions. In addition, since the instabilities shown in our models are purely voltage-driven, constant-DI pacing may not be appropriate in differentiating voltage-driven instabilities from Ca^{2+} -driven instabilities as suggested by Cherry.²¹

Finally, we would like to point out that we only studied two sources of memory: the slow recovery of the K^+ channel and the slow accumulation of intracellular Ca^{2+} concentration. However, there are many sources of memory in the heart, from seconds to minutes. Memory from the K^+ channel is due to the slow component of the delayed K^+ current I_{Ks} ,^{57–59} which activates and recovers slowly on the order of several

hundred milliseconds to a couple of seconds. The memory effect in the LR1 model is mainly caused by the K^+ current, which only takes a couple of beats to recover after a sudden change in the pacing period (Fig. S1). Another major source of memory is from the slow accumulation of intracellular ion (Na^+ , K^+ , and Ca^{2+}) concentrations, which can take minutes to re-equilibrate after a sudden change in heart rate.⁶⁰ In our study of the TP04 model, since we set Na^+ to be a constant, the memory effect is caused only by Ca^{2+} accumulation which takes 10 to 20 beats (i.e., 10 to 20 s) to reach steady state after a sudden change in the pacing period (Fig. S2). In the experimental study by Franz *et al.*,⁶¹ it took about 120 s for the APD to reach a new steady state after a sudden change in the pacing period. In a series of experimental studies by Kunsyż *et al.*,^{62–64} they showed that in spontaneous beating chicken heart aggregates, it took tens of seconds for the aggregates to go back to steady state after overdrive pacing. The memory time constant in the TP04 model is in the same order of magnitude as in the experiments despite the exclusion of memory from Na^+ accumulation. If Na^+ is not clamped in the TP04 model, the time constant of memory will be significantly longer. Recent studies have shown that slow accumulation may also promote interesting action potential dynamics.^{65,66} As shown in our general iterated map analyses, it will be more difficult to control the instabilities for a longer memory time constant. Although in theory the NFC method that we propose in this study is able to control the instabilities when the memory effect is strong, it may depend too sensitively on the strength of control signal to be practically useful (see Fig. S5). Therefore, better control algorithms are needed for the control of the instabilities under the diseased conditions in which strong memory effects exist.

SUPPLEMENTARY MATERIAL

See [supplementary material](#) for further supporting figures. Figures S1 and S2 demonstrate the duration of memory in the LR1+ I_{to} and TP04 models. Figures S3–S5 show the effectiveness of controlling APD instability due to slow Ca^{2+} concentration accumulation in the TP04 model. Figures S6 and S7 show the effectiveness of controlling APD instability in the LR1 model under the condition of EADs.

ACKNOWLEDGMENTS

This work was supported by National Institutes of Health under Grant Nos. R01 HL133294 and T32-GM008185 (to J.L.). The authors thank J. N. Weiss, A. Garfinkel, and other members of the UCLA arrhythmia group for useful comments and feedback.

¹L. Glass, “Dynamics of cardiac arrhythmias,” *Phys. Today* **49**(8), 40–45 (1996).

²Z. Qu, G. Hu, A. Garfinkel, and J. Weiss, “Nonlinear and stochastic dynamics in the heart,” *Phys. Rep.* **543**, 61–162 (2014).

³T. Krogh-Madsen and D. J. Christini, “Nonlinear dynamics in cardiology,” *Annu. Rev. Biomed. Eng.* **14**, 179–203 (2012).

⁴A. Karma, “Physics of cardiac arrhythmogenesis,” *Annu. Rev. Condens. Matter Phys.* **4**, 313–337 (2013).

⁵A. Garfinkel, M. L. Spano, W. L. Ditto, and J. N. Weiss, “Controlling cardiac chaos,” *Science* **257**, 1230–1235 (1992).

⁶D. J. Christini and J. J. Collins, “Using chaos control and tracking to suppress a pathological nonchaotic rhythm in a cardiac model,” *Phys. Rev. E* **53**, R49 (1996).

⁷W. L. Ditto, M. L. Spano, V. In, J. Neff, B. Meadows, J. Langberg, A. Bolmann, and K. McTeague, “Control of human atrial fibrillation,” *Int. J. Bifurcat. Chaos* **10**, 593–601 (2000).

⁸D. J. Christini, M. L. Riccio, C. A. Cuiianu, J. J. Fox, A. Karma, and R. F. Gilmour, Jr., “Control of electrical alternans in canine cardiac purkinje fibers,” *Phys. Rev. Lett.* **96**, 104101 (2006).

⁹G. M. Hall and D. J. Gauthier, “Experimental control of cardiac muscle alternans,” *Phys. Rev. Lett.* **88**, 198102 (2002).

¹⁰K. Hall, D. J. Christini, M. Tremblay, J. J. Collins, L. Glass, and J. Billette, “Dynamic control of cardiac alternans,” *Phys. Rev. Lett.* **78**, 4518 (1997).

¹¹W.-J. Rappel, F. Fenton, and A. Karma, “Spatiotemporal control of wave instabilities in cardiac tissue,” *Phys. Rev. Lett.* **83**, 456 (1999).

¹²E. G. Tolkacheva, M. M. Romeo, M. Guerraty, and D. J. Gauthier, “Condition for alternans and its control in a two-dimensional mapping model of paced cardiac dynamics,” *Phys. Rev. E* **69**, 031904 (2004).

¹³T. Krogh-Madsen, A. Karma, M. L. Riccio, P. N. Jordan, D. J. Christini, and R. F. Gilmour, Jr., “Off-site control of repolarization alternans in cardiac fibers,” *Phys. Rev. E* **81**, 011915 (2010).

¹⁴D. J. Christini, K. M. Stein, S. M. Markowitz, S. Mittal, D. J. Slotwiner, M. A. Scheiner, S. Iwai, and B. B. Lerman, “Nonlinear-dynamical arrhythmia control in humans,” *Proc. Natl. Acad. Sci. U.S.A.* **98**, 5827–5832 (2001).

¹⁵B. Echebarria and A. Karma, “Spatiotemporal control of cardiac alternans,” *Chaos* **12**, 923–930 (2002).

¹⁶A. A. Armoundas, E. H. Weiss, O. Sayadi, S. Laferriere, N. Sajja, T. Mela, J. P. Singh, C. D. Barrett, E. K. Heist, and F. M. Merchant, “A novel pacing method to suppress repolarization alternans in vivo: Implications for arrhythmia prevention,” *Heart Rhythm* **10**, 564–572 (2013).

¹⁷P. N. Jordan and D. J. Christini, “Adaptive diastolic interval control of cardiac action potential duration alternans,” *J. Cardiovasc. Electrophysiol.* **15**, 1177–1185 (2004).

¹⁸R. Wu and A. Patwardhan, “Restitution of action potential duration during sequential changes in diastolic intervals shows multimodal behavior,” *Circ. Res.* **94**, 634–641 (2004).

¹⁹R. Wu and A. Patwardhan, “Mechanism of repolarization alternans has restitution of action potential duration dependent and independent components,” *J. Cardiovasc. Electrophysiol.* **17**, 87–93 (2006).

²⁰S. D. McIntyre, V. Kakade, Y. Mori, and E. G. Tolkacheva, “Heart rate variability and alternans formation in the heart: The role of feedback in cardiac dynamics,” *J. Theor. Biol.* **350**, 90–97 (2014).

²¹E. M. Cherry, “Distinguishing mechanisms for alternans in cardiac cells using constant-diastolic-interval pacing,” *Chaos* **27**, 093902 (2017).

²²N. F. Otani, “Theory of the development of alternans in the heart during controlled diastolic interval pacing,” *Chaos* **27**, 093935 (2017).

²³S. Zlochiver, C. Johnson, and E. G. Tolkacheva, “Constant di pacing suppresses cardiac alternans formation in numerical cable models,” *Chaos* **27**, 093903 (2017).

²⁴M. Guevara, G. Ward, A. Shrier, and L. Glass, “Electrical alternans and period doubling bifurcations,” *IEEE Comput. Cardiol.* **562**, 167–170 (1984).

²⁵J. Nolasco and R. Dahlen, “A graphic method for the study of alternation in cardiac action potentials,” *J. Appl. Physiol.* **25**, 191–196 (1968).

²⁶Z. Qu, Y. Shiferaw, and J. N. Weiss, “Nonlinear dynamics of cardiac excitation-contraction coupling: An iterated map study,” *Phys. Rev. E* **75**, 011927 (2007).

²⁷Y. Shiferaw, D. Sato, and A. Karma, “Coupled dynamics of voltage and calcium in paced cardiac cells,” *Phys. Rev. E* **71**, 021903 (2005).

²⁸Z. Qu, “Nonlinear dynamic control of irregular cardiac rhythms,” *J. Cardiovasc. Electrophysiol.* **15**, 1186–1187 (2004).

²⁹E. Chudin, J. Goldhaber, A. Garfinkel, J. Weiss, and B. Kogan, “Intracellular Ca^{2+} dynamics and the stability of ventricular tachycardia,” *Biophys. J.* **77**, 2930–2941 (1999).

³⁰M. Diaz, D. Eisner, and S. O’Neill, “Depressed ryanodine receptor activity increases variability and duration of the systolic Ca^{2+} transient in rat ventricular myocytes,” *Circ. Res.* **91**, 585–593 (2002).

³¹M. E. Diaz, S. C. O’Neill, and D. A. Eisner, “Sarcoplasmic reticulum calcium content fluctuation is the key to cardiac alternans,” *Circ. Res.* **94**, 650–656 (2004).

- ³²D. R. Chialvo, R. F. Gilmour, Jr., and J. Jalife, "Low dimensional chaos in cardiac tissue," *Nature* **343**, 653–657 (1990).
- ³³N. F. Otani and R. F. Gilmour, Jr., "Memory models for the electrical properties of local cardiac systems," *J. Theor. Biol.* **187**, 409–436 (1997).
- ³⁴J. J. Fox, E. Bodenschatz, and R. F. Gilmour, Jr., "Period-doubling instability and memory in cardiac tissue," *Phys. Rev. Lett.* **89**, 138101 (2002).
- ³⁵E. G. Tolkacheva, D. G. Schaeffer, D. J. Gauthier, and W. Krassowska, "Condition for alternans and stability of the 1:1 response pattern in a 'memory' model of paced cardiac dynamics," *Phys. Rev. E* **67**, 031904 (2003).
- ³⁶S. S. Kalb, E. G. Tolkacheva, D. G. Schaeffer, D. J. Gauthier, and W. Krassowska, "Restitution in mapping models with an arbitrary amount of memory," *Chaos* **15**, 023701 (2005).
- ³⁷J. J. Fox, M. L. Riccio, P. Drury, A. Werthman, and R. F. Gilmour, Jr., "Dynamic mechanism for conduction block in heart tissue," *New J. Phys.* **5**, 101 (2003).
- ³⁸E. M. Cherry and F. H. Fenton, "Suppression of alternans and conduction blocks despite steep apd restitution: Electrotonic, memory, and conduction velocity restitution effects," *Am. J. Physiol.* **286**, H2332–H2341 (2004).
- ³⁹A. Baher, Z. Qu, A. Kayatdavoudi, S. T. Lamp, M.-J. Yang, F. Xie, S. Turner, A. Garfinkel, and J. N. Weiss, "Short-term cardiac memory and mother rotor fibrillation," *Am. J. Physiol. Heart Circ. Physiol.* **292**, H180–H189 (2007).
- ⁴⁰D. G. Schaeffer, J. W. Cain, D. J. Gauthier, S. S. Kalb, R. A. Oliver, E. G. Tolkacheva, W. Ying, and W. Krassowska, "An ionically based mapping model with memory for cardiac restitution," *Bull. Math. Biol.* **69**, 459–482 (2007).
- ⁴¹A. Gizzi, E. Cherry, R. F. Gilmour, Jr., S. Luther, S. Filippi, and F. H. Fenton, "Effects of pacing site and stimulation history on alternans dynamics and the development of complex spatiotemporal patterns in cardiac tissue," *Front. Physiol.* **4**, 71 (2013).
- ⁴²S. Mironov, J. Jalife, and E. G. Tolkacheva, "Role of conduction velocity restitution and short-term memory in the development of action potential duration alternans in isolated rabbit hearts," *Circulation* **118**, 17–25 (2008).
- ⁴³N. Wei, Y. Mori, and E. G. Tolkacheva, "The role of short term memory and conduction velocity restitution in alternans formation," *J. Theor. Biol.* **367**, 21–28 (2015).
- ⁴⁴J. Sun, F. Amellal, L. Glass, and J. Billette, "Alternans and period-doubling bifurcations in atrioventricular nodal conduction," *J. Theor. Biol.* **173**, 79–91 (1995).
- ⁴⁵J. Landaw, A. Garfinkel, J. N. Weiss, and Z. Qu, "Memory-induced chaos in cardiac excitation," *Phys. Rev. Lett.* **118**, 138101 (2017).
- ⁴⁶J. Landaw and Z. Qu, "Memory-induced nonlinear dynamics of excitation in cardiac diseases," *Phys. Rev. E* **97**, 042414 (2018).
- ⁴⁷C. Antzelevitch and G.-X. Yan, "J-wave syndromes: Brugada and early repolarization syndromes," *Heart Rhythm* **12**, 1852–1866 (2015).
- ⁴⁸D. M. Roden, "Long-qt syndrome," *New Engl. J. Med.* **358**, 169–176 (2008).
- ⁴⁹D. M. Roden, "Long QT syndrome: Reduced repolarization reserve and the genetic link," *J. Intern. Med.* **259**, 59–69 (2006).
- ⁵⁰G.-R. Li, C.-P. Lau, A. Ducharme, J.-C. Tardif, and S. Nattel, "Transmural action potential and ionic current remodeling in ventricles of failing canine hearts," *Am. J. Physiol. Heart Circ. Physiol.* **283**, H1031–H1041 (2002).
- ⁵¹G.-R. Li, C.-P. Lau, T.-K. Leung, and S. Nattel, "Ionic current abnormalities associated with prolonged action potentials in cardiomyocytes from diseased human right ventricles," *Heart Rhythm* **1**, 460–468 (2004).
- ⁵²G. F. Tomaselli and D. P. Zipes, "What causes sudden death in heart failure?," *Circ. Res.* **95**, 754–763 (2004).
- ⁵³C.-H. Luo and Y. Rudy, "A model of the ventricular cardiac action potential. Depolarization, repolarization, and their interaction," *Circ. Res.* **68**, 1501–1526 (1991).
- ⁵⁴A. Mahajan, Y. Shiferaw, D. Sato, A. Baher, R. Olcese, L.-H. Xie, M.-J. Yang, P.-S. Chen, J. G. Restrepo, A. Karma *et al.*, "A rabbit ventricular action potential model replicating cardiac dynamics at rapid heart rates," *Biophys. J.* **94**, 392–410 (2008).
- ⁵⁵A model for human ventricular tissue," *Am. J. Physiol. Heart Circ. Physiol.* **286**, H1573–H1589 (2004).
- ⁵⁶Z. Qu and J. N. Weiss, "Mechanisms of ventricular arrhythmias: From molecular fluctuations to electrical turbulence," *Annu. Rev. Physiol.* **77**, 29–55 (2015).
- ⁵⁷M. C. Sanguinetti and N. K. Jurkiewicz, "Two components of cardiac delayed rectifier k⁺ current. Differential sensitivity to block by class iii antiarrhythmic agents," *J. Gen. Physiol.* **96**, 195–215 (1990).
- ⁵⁸J. Zeng, K. R. Laurita, D. S. Rosenbaum, and Y. Rudy, "Two components of the delayed rectifier k⁺ current in ventricular myocytes of the guinea pig type," *Circ. Res.* **77**, 140–152 (1995).
- ⁵⁹J. Silva and Y. Rudy, "Subunit interaction determines its participation in cardiac repolarization and repolarization reserve," *Circulation* **112**, 1384–1391 (2005).
- ⁶⁰G. M. Faber and Y. Rudy, "Action potential and contractility changes in [na⁺]_i overloaded cardiac myocytes: A simulation study," *Biophys. J.* **78**, 2392–2404 (2000).
- ⁶¹M. R. Franz, C. D. Swerdlow, L. B. Liem, and J. Schaefer, "Cycle length dependence of human action potential duration in vivo. Effects of single extrastimuli, sudden sustained rate acceleration and deceleration, and different steady-state frequencies," *J. Clin. Invest.* **82**, 972–979 (1988).
- ⁶²A. M. Kunysz, L. Glass, and A. Shrier, "Overdrive suppression of spontaneously beating chick heart cell aggregates: Experiment and theory," *Am. J. Physiol. Heart Circ. Physiol.* **269**, H1153–H1164 (1995).
- ⁶³A. M. Kunysz, A. A. Munk, and A. Shrier, "Phase resetting and dynamics in isolated atrioventricular nodal cell clusters," *Chaos* **5**, 184–192 (1995).
- ⁶⁴A. M. Kunysz, A. Shrier, and L. Glass, "Bursting behavior during fixed-delay stimulation of spontaneously beating chick heart cell aggregates," *Am. J. Physiol. Cell Physiol.* **273**, C331–C346 (1997).
- ⁶⁵Y. Xie, Z. Liao, E. Grandi, Y. Shiferaw, and D. M. Bers, "Slow [Na]_i changes and positive feedback between membrane potential and [Ca]_i underlie intermittent early afterdepolarizations and arrhythmias," *Circ. Arrhythm. Electrophysiol.* **8**, 1472–1478 (2015).
- ⁶⁶T. Krogh-Madsen and D. J. Christini, "Slow [Na⁺]_i dynamics impacts arrhythmogenesis and spiral wave reentry in cardiac myocyte ionic model," *Chaos* **27**, 093907 (2017).